ISSN 1560-0904, Polymer Science, Series B, 2022, Vol. 64, No. 6, pp. 841–854. © Pleiades Publishing, Ltd., 2022.
ISSN 1560-0904, Polymer Science, Series B, 2022. © Pleiades Publishing, Ltd., 2022.
Russian Text © The Author(s), 2022, published in Vysokomolekulyarnye Soedineniya, Seriya B, 2022, Vol. 64, No. 6, pp. 435–449.

FUNCTIONAL POLYMERS

Synthesis and Thermal and Phase Behavior of Polysiloxanes with Grafted Dialkyl-Substituted [1]Benzothieno[3,2-b][1]benzothiophene Groups

E. A. Zaborin[a], O. V. Borshchev[a], M. S. Skorotetskii[a], V. V. Gorodov[a], A. V. Bakirov[a], M. S. Polinskaya[a], S. N. Chvalun[a], and S. A. Ponomarenko[a,*]

[a] *Enikolopov Institute of Synthetic Polymer Materials, Russian Academy of Sciences, Moscow, 117393 Russia*

**e-mail: ponomarenko@ispm.ru*

Received July 4, 2022; revised September 13, 2022; accepted September 20, 2022

Abstract—A number of novel polysiloxanes with grafted dialkyl-substituted [1]benzothieno[3,2-b][1]benzothiophene groups is synthesized by the hydrosilylation of polymethylsiloxane matrices with varying ratio of functional methylsiloxane and nonfunctional dimethylsiloxane fragments (1 : 5, 1 : 1, and 1 : 0) by reactive 2-undecenyl-7-hexyl-[1]benzothieno[3,2-b][1]benzothiophene. The obtained comb-shaped polymers have a number-average molecular weight of (6–43) × 10^3 and a dispersity of 1.55–2.79. Study of the thermal and thermo-oxidative properties shows that the polymer, in which each second monomer unit contains [1]benzothieno[3,2-b][1]benzothiophene substituents, has the highest thermo-oxidative stability (413°C) and the smallest char residue at 700°C (3%). The lowest thermal stability is exhibited by the comb-shaped polymer with the 100% content of [1]benzothieno[3,2-b][1]benzothiophene fragments and the highest molecular weight for which a 5% weight loss starts at 274°C. The DSC study of the phase behavior of the synthesized polymers indicates that increase in the fraction of [1]benzothieno[3,2-b][1]benzothiophene fragments in monomer units and their molecular weight contributes to a rise in phase transition temperatures and reduction in their enthalpy compared with the monomer and the siloxane dimer of [1]benzothieno[3,2-b][1]benzothiophene. Introduction of 50 and 100% of [1]benzothieno[3,2-b][1]benzothiophene fragments into the siloxane polymer chain leads to the formation of liquid-crystalline mesophases with the enthalpy of transitions typical of smectics, as evidenced by polarizing microscopy and X-ray diffraction. For the polymers with the varied content of [1]benzothieno[3,2-b][1]benzothiophene fragments the values of the interlayer spacing in the smectic mesophase are determined, and their phase behavior is investigated. Effect of molecular weight on the packing of [1]benzothieno[3,2-b][1]benzothiophene is ascertained, and models for the interpenetration of side substituents in the obtained polymers are constructed.

DOI: 10.1134/S1560090422700427

INTRODUCTION

Organic and polymer semiconductors are the topical subject of research primarily due to their unique electrical and optical properties combined with good solubility in organic solvents, flexibility of devices based on them, and low-cost technology of their manufacturing [1]. Organic semiconductors are used in organic field-effect transistors, organic light emitting diodes, biosensors, organic solar cells, etc. [2–4]. The research of organic semiconductors is ongoing both in the field of synthesis of novel materials and in terms of improving technology of manufacturing various devices designed on their basis.

[1]Benzothieno[3,2-b][1]benzothiophene (**BTBT**) and its derivatives are among the most effective organic semiconductors applied in organic field-effect transistors [5, 6]. Various BTBT derivatives are used as functional materials in diverse organic electronic devices: from organic field-effect transistors [7–9] to phototransistors [10], as well as nonfullerene acceptors in organic solar cells [11, 12]. Effect of the number of carbon atoms (the even-odd effect) in alkyl- and alkoxy-substituted BTBTs on the packing of supramolecular structures and thermal and electrical properties of organic semiconductors based on them was investigated [13]. The authors of [14, 15] studied difference in the physicochemical properties of mono- and disubstituted alkyl derivatives of BTBT. Organic field-effect transistors based on asymmetric alkylnaphthyl derivatives of BTBT possess good electrical properties [16]. Thin films of asymmetric decylphenyl BTBT show good solubility and high hole mobility—up to 1.3 $cm^2/(V\,s)$ [17].

However, until recently insufficient attention has been paid to polymer materials containing conjugated BTBT fragments. It is mostly focused on molecules, in which the conjugated fragment occurs in the polymer

backbone. Copolymers containing BTBT, 9,9-didecylfluorene, and 4,7-dithiophen-2-yl-benzo(3,1,2)thiadiazole fragments at various ratios were prepared by the organometallic synthesis reaction under the Suzuki conditions [18]. Investigation of their optical, electrochemical, and photovoltaic properties demonstrated that the presence of even a small number of BTBT fragments in macromolecules causes a gain in the efficiency of solar cells based on these copolymers. Organic field-effect transistors based on BTBT copolymers with arylenediimides demonstrated a high mobility of charge carriers for a number of perylene diimide polymers, thereby confirming the efficiency of introducing BTBT fragments into the polymer chain in order to improve the efficiency of electronic devices based on them [19]. Studies of organic field-effect transistors based on the copolymer of BTBT, thiophene, and diketopyrrole showed that with increasing amount of BTBT fragments in the polymer chain the hole conductivity grows to 2.47 $cm^2/(V\ s)$ [20]. The same authors reported that an increase in the number of BTBT fragments insignificantly affects the optical properties of films and solutions obtained using these polymers.

Organosilicon derivatives of BTBT are currently known only in the form of siloxane dimers [21]. These novel organic electronic materials possess, in addition to great hole charge-carrier mobility, high thermal stability, air stability, and good solubility in common organic solvents [22]. The unique structure of these compounds combines BTBT fragments exhibiting good semiconductor properties with flexible alkyl spacers markedly improving solubility. Owing to the presence of siloxane moieties, self-assembled multilayer organic field-effect transistors applied as chemosensors of toxic gases can be manufactured [23].

This paper presents the data on the synthesis and properties of novel polysiloxanes modified with dialkyl derivatives of BTBT; their chemical formulas and schematic structure are outlined below.

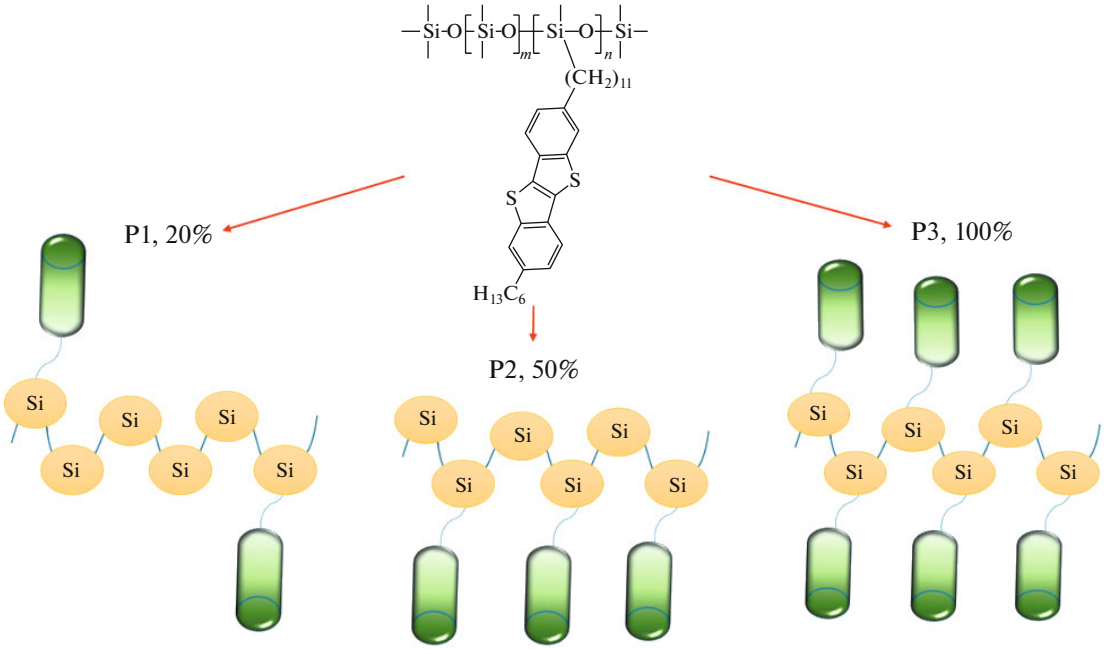

Polysiloxanes containing different number of functional silyl hydride fragments, to which 2-undecyl-11-en-7-hexyl [1]benzothieno[3,2-b] [1]benzothiophene fragments were added through the hydrosilylation reaction, were used as a polymer matrix. The obtained polymers were investigated by thermogravimetric and differential calorimetric analyses. Their phase behavior was studied by polarizing optical microscopy.

EXPERIMENTAL

Gel permeation chromatography (GPC) analysis was carried out on a Shimadzu chromatography system equipped with a RID10AVP refractometer, an SPD-M10AVP diode matrix, and columns 300 mm in length and 7.8 mm in diameter (300 mm × 7.8 mm) (Phenomenex, United States) filled with the Phenogel sorbent (Phenomenex, United States) having a particle size of 5 μm and a pore size of 500 Å; the system consisting of a Stayer s. 2 high-pressure pump (Akvilon, Russia), a SmartlineRI 2300 refractometric detector (Knauer, Germany), and a JETSTREAM 2 PLUS column thermostat (Knauer, Germany) was used. The thermostat temperature was 40 ± 0.1°C, and THF at a flow rate of 1.0 mL/min was used as an eluent. The results of analysis were processed with the

help of the program MultiKhrom 1.6 GPC (Ampersend, Russia) using polystyrene standards. Preparative GPC separation was performed on a Shimadzu system equipped with a RID10A refractometer, an SPD-M20A diode matrix, and columns (300 mm x 21.2 mm) (Phenomenex, United States) filled with the Phenogel sorbent (Phenomenex, United States) having a pore size of 10^4 Å. The thermostat temperature was 40 ± 0.1°C, and THF was used as an eluent.

Thermal properties were analyzed in the temperature range of −150...+270°C by differential scanning calorimetry (DSC) using a Mettler Toledo DSC30 instrument (United States) under a nitrogen flow rate of 50 mL/min and at a scan rate of 20 deg/min. Thermogravimetric analysis was performed on a Mettler Toledo TG50 instrument (United States) at an air and nitrogen flow rate of 200 mL/min.

Small-angle and wide-angle X-ray diffraction patterns were recorded on a Hecus S3-Micropix system (CuK_α-radiation, λ = 1.542Å) with a high voltage and current on a Xenocs Genix source tube of 50 kV and 1 mA, respectively. A Dectris Pilatus 100K detector and a linear PSD detector for wide-angle measurements were used. A Fox 3D X-ray optics was employed to generate the X-ray beam, and the diameter of Kratky collimation slits was 0.1 and 0.2 mm, respectively. The range of diffraction angle measurements was 0.05–19.0 nm^{-1}. The temperature of the sample in the thermostatted accessory was varied from room temperature to 300°C with an accuracy of 1°C. The exposure time was 3000 s, and calibration was done against the silver behenate standard. ^{1}H NMR spectra were measured on a Bruker WP-250 SY spectrometer (United States) at a frequency of 250 MHz, with the chloroform signal at 7.25 ppm being used as an internal standard. Phase behavior was studied on a Carl Zeiss Axioscop A40Pol polarizing optical microscope (Germany).

The technique of synthesis of initial polydimethylmethylhydroxysiloxanes (**PMS**) containing 20% (**PMS20**) and 50% (**PMS50**) Si–H groups was described in [24]. Commercial product of the Penta-804 trademark (Russia) was used as polymethylhydrosiloxane (**PMS100**) containing the silyl hydride function in each unit. [1]Benzothieno[3,2-b] [1]benzothiene-2-yl)-hexanone (**2**) was prepared according to the technique described in [16]. 10,11-Dibromo-1-(7-hexyl [1]benzothieno[3,2-b] [1]benzothiene-2-yl)undecanone (**4**) was synthesized by the Friedel–Crafts acylation reaction as described in [21].

2-Hexyl-[1]benzothieno[3,2-b][1]benzothiophene (**3**) was obtained by the Wolff–Kizhner reaction. A 1 L two-neck flask was loaded with 1.57 g (4.63 mmol) of compound 2, 0.94 g (16.7 mmol) of KOH, 3.6 mL of 80% hydrazine hydrate, and 200 mL of ethylene glycol. The reaction mixture was refluxed under stirring for 5 h, and the reaction was monitored by thin-layer chromatography using toluene as an eluent. The reaction mixture was cooled to room temperature and extracted from the aqueous phase by diethyl ether. The organic phase was concentrated on a rotor evaporator and dried on an oil pump to remove residual organic solvents. The crude compound was purified by column chromatography using cyclohexane as an eluent. After purification and drying, the yield of the target product was 1.26 g (84%).

2-Hexyl-7-undecenyl[1]benzothieno[3,2-b][1]benzothiophene (**5**) was obtained by the reduction of compound 4 using $LiAlH_4$ as a reducing agent. A 250 mL two-neck flask containing 1 g (1.53 mmol) of compound 4 was loaded with 80 mL of dry diethyl ether and 0.9 g (23.7 mmol) $LiAlH_4$, and then 0.4 g (3 mmol) of anhydrous $AlCl_3$ was carefully added. The reaction mixture was refluxed under stirring for 40 h, and the reaction was monitored by TLC in toluene. When the reaction was completed, the reaction mixture was carefully quenched with distilled water; the flask was precooled by placing in an ice bath. The reaction mixture was extracted from the aqueous phase by diethyl ether. The organic phase was concentrated on the rotor evaporator and dried on the oil pump to remove residual organic solvents. The crude compound was purified by column chromatography using first toluene and then cyclohexane as eluents. After all purification procedures the yield of the product was 290 mg (40%).

Synthesis of Polymer P1. The Hydrosilylation Reaction

A flask was loaded in an inert atmosphere with a solution of organosilicon polymer PMS20 (148 mg) in 10 mL of dry toluene, the reaction mixture was heated to 90°C, and a solution of compound 5 (220 mg, 0.46 mmol) in 10 mL of dry toluene and 25 μL of Karstedt's catalyst were added dropwise. After stirring for 13 h at 90°C the reaction mixture was passed through a silica gel layer in toluene. The mixture was concentrated on the rotor evaporator and dried on the oil pump. The target polymer P1 was purified on a preparative chromatograph. After purification and drying, the yield of the product was 102 mg (35%). ^{1}H NMR (250 MHz, $CDCl_3$, δ, ppm): 0,09 (m, 52H), 0,49 (m, 3H), 0,89 (s, 4H), 1.31 (d, 26 H, J = 18.34 Hz), 1.68 (m, 5H), 2,74 (m, 4H), 7.23 (m, 2H), 7,72 (m, 4H).

Synthesis of Polymer P2

Synthesis was conducted according to the technique described above for polymer P1 through the interaction of organosilicon polymer PMS50 (80 mg), compound 5 (270 mg, 0.56 mmol), and 25 μL of Karstedt's catalyst in 90 mL of dry toluene. The reaction was carried out for 3 h. The target polymer P2 was purified on the preparative gel permeation chromatograph. After purification and drying the yield of the

product was 59 mg (15%). ^{1}H NMR (250 MHz, $CDCl_3$, δ, ppm.): 0.05 (m, 20H), 0.49 (m, 3H), 0.86 (s, 4H), 1.25 (d, 24H, J = 10.99 Hz), 1.67 (m, 4H), 2.68 (m, 4H), 7.14 (m, 2H), 7.64 (m, 4H).

Synthesis of Polymer P3

Polymer P3 was synthesized according to the technique described above for polymer P1 through the interaction of organosilicon polymer PMS100 (31 mg), compound 5 (260 mg, 0.55 mmol), and 25 μL of Karstedt's catalyst in 20 mL of dry toluene for 2 h. The target polymer P3 was fractionated on the preparative GPC to afford 26 mg of **P3a** (yield, 11%) and 40 mg of **P3b** (yield, 17%). P3a: ^{1}H NMR (250 MHz, $CDCl_3$, δ, ppm): 0.06 (m, 10H), 0.5 (m, 2H), 0.84 (s, 10H), 1.24 (s, 34H), 1.56 (s, 10H), 2.6 (m, 4H), 7.01 (s, 2H), 7.54 (m, 4H). P3b: ^{1}H NMR (250 MHz, $CDCl_3$, δ, ppm): 0.06 (m, 6H), 0.48 (m, 2H), 0.84 (s, 4H), 1.24 (s, 22H), 1.59 (s, 6H), 2.62 (m, 4H), 7.08 (s, 2H), 7.57 (m, 4H).

RESULTS AND DISCUSSION

To ascertain effect of the fraction of grafted BTBT fragments on the phase behavior and properties of target macromolecules organosilicon polymers containing 20 and 50% of Si–H reactive groups (PMS20 and PMS50, respectively) were used. Polydimethylsiloxane PMS100 was chosen as a polymer bearing the silyl hydride function in each unit (100%).

For the synthesis of novel polysiloxanes modified with dialkyl derivatives of BTBT the reaction of hydrosilylation between PMS and asymmetric dialkyl derivative of BTBT (5) containing the end double bond in the undecylenic group was chosen as the key reaction.

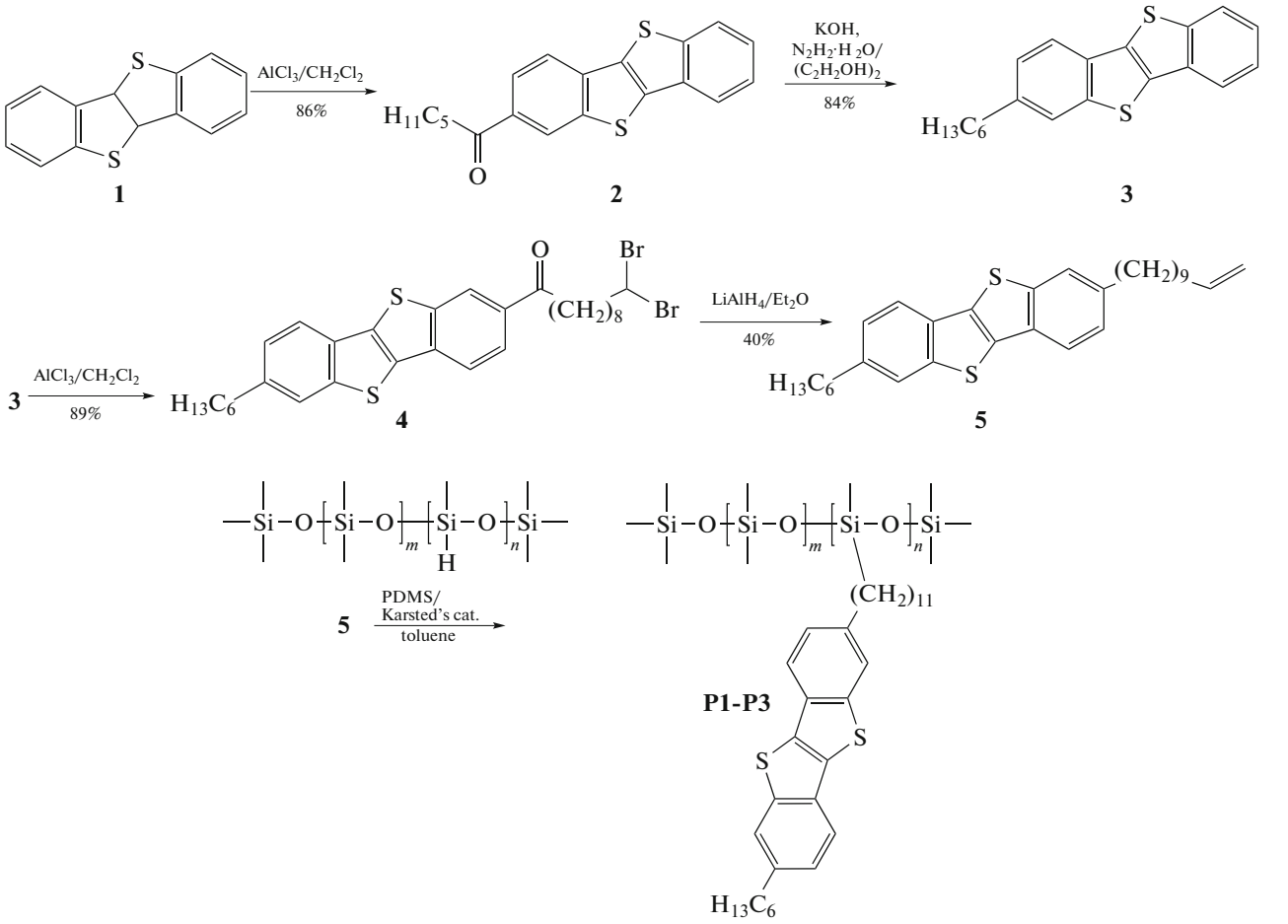

This choice was associated with the accessibility of reactants and the possibility to easily track progress of the reaction by monitoring the disappearance of ^{1}H NMR signals due to protons in $-CH=CH_2$ (characteristic multiplets at 4.96 and 5.8 ppm) and Si–H fragments (multiplet at 4.7 ppm) (Fig. 1).

The synthesis of 2-hexyl-(7-undec-10-en-1-yl) [1]benzothieno[3,2-b] [1]benzothiophene (5) consists of four stages involving the sequential addition of acid chlorides in positions 2 and 7 of BTBT (**1**) through the Friedel–Crafts acylation and further reduction of the resulting ketones.

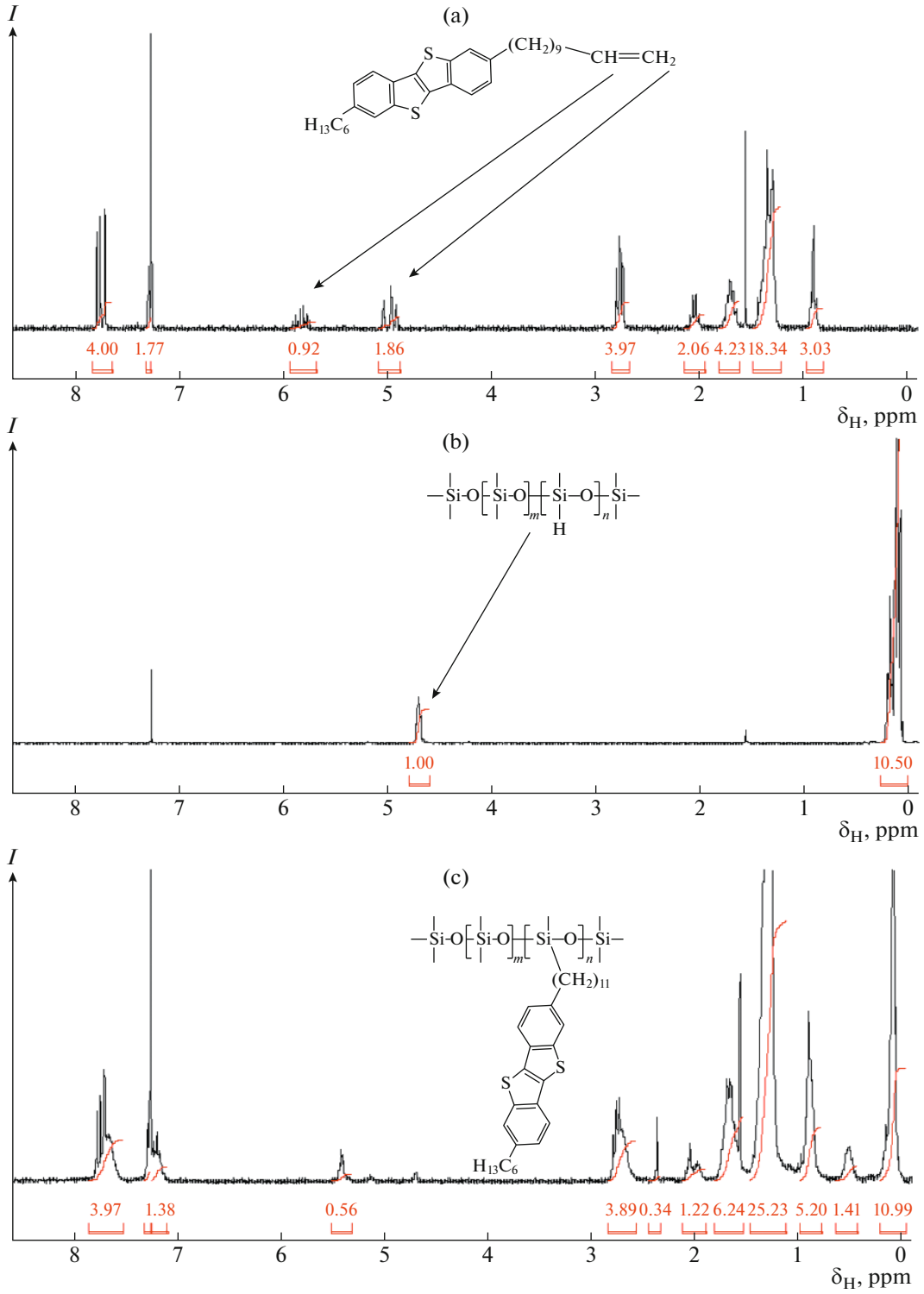

Fig. 1. NMR spectra of (a) compound 5, (b) copolymer PMS50, and (c) the reaction mixture in the synthesis of copolymer P2. Color figures are available in the electronic version.

At the first step BTBT was acylated by hexanoyl chloride according to [16] to afford [1]benzothieno[3,2-b] [1]benzothiene-2-yl)-hexanone (**2**) with a yield of 86%. This compound was reduced via the Wolff–Kizhner reaction using hydrazine hydrate in the presence of potassium hydroxide in ethylene glycol to afford the alkyl derivative of BTBT (**3**) with a yield of 84%. The advantages of the proposed method for

Table 1. Molecular weight characteristics of polymers P1–P3

Polymer	$M_n \times 10^{-3}$	$M_w \times 10^{-3}$	Dispersity D
P1	12.3	33.6	2.73
P2	21.1	42.2	2.00
P3a	43.1	120.0	2.79
P3b	6.0	9.3	1.55

the synthesis of compound 3 over the previously described method of reducing compound 2 by sodium borohydride are higher reaction rate and yield. Compound 3 was introduced in the reaction of acylation with 10,11-dibromoundecanoyl chloride used as an acylating agent. Ketone 4 obtained with a yield of 89% was reduced by $LiAlH_4$ in diethyl ether [25]. Note that in the latter reaction, along with reduction of the keto group, dibromide deprotection occurred to give rise to the target asymmetric dialkyl derivative of BTBT (5) with the end double bond. Previously described synthesis of compound 5 involved the sequential reduction of compound 3 by sodium borohydride and subsequent dibromide deprotection by metal zinc with a total yield of 69% [21]. An attempt to reduce ketone 4 by the Wolff–Kizhner reaction failed due to formation of many side products.

Compound 5 was introduced in the hydrosilylation reaction with various PMSs in the presence of Karstedt's catalyst in anhydrous toluene at 90°C. After the reaction for 2 h, the ^{1}H NMR spectrum of the sample taken from the reaction mixture showed no signals due to protons in the end double bond and signal due to proton at silicon in Si–H, indicating the complete consumption of reactive groups. According to the GPC analysis, the reaction mixture contained a small amount of unreacted BTBT derivative which is related to transfer of the multiple bond of undecenyl fragment from position 10 of the carbon chain to position 9 characterized by the ^{1}H NMR signal at 5.4 ppm [26]. Therefore, all synthesized polymers were purified from the side product by preparative GPC. Polymer P3 was fractionated into two fractions: high molecular weight P3a and low molecular weight P3b. An analytical GPC analysis of the polymers with the use of polystyrene standards showed that their number-average molecular weights M_n varied in the range of (6.0–43.1) $\times 10^3$ and dispersity ranged from 1.55 to 2.79 (Table 1).

The TGA results indicate that all synthesized polymers possess high thermal and thermo-oxidative stability: a 5% weight loss for polymers P1, P2, and P3b starts at temperatures above 390°C in an atmosphere of nitrogen and 325°C in air (Table 2). Polymer P3a with the highest molecular weight exhibits the lowest thermal stability: its 5% weight loss starts at 274°C in both media (Fig. 2). The maximum char residue (24% at 700°C) in an atmosphere of nitrogen is observed for polymers P3a and P3b with BTBT substituents in each monomer unit, that is, with the highest content of polyaromatic fragments. The amount of the char residue at 700°C in air decreases in the sequence P1–P3b–P3a–P2 (29, 24, 17, and 3%). It is interesting that polymer P2, in which each second monomer unit contains BTBT substituents, exhibits the highest thermo-oxidative stability (413°C) and, at the same time, the smallest char residue at 700°C (3%).

The first and second heating DSC thermograms of polymer P1 show baseline inflectionsat –128 and –96°C, respectively, which correspond to the devitrification of siloxane fragments in the main polymer chain (Fig. 3) [27]. Furthermore, there are broad endothermic peaks with maxima at 50 and 110°C and a melting enthalpy of 12–18 and 6 J/g, respectively. As follows from polarizing optical microscopy, for polymer P1 in crossed polaroids birefringence is observed at room temperature. The intensity of birefringence gradually decreases under heating and disappears above 120°C (Fig. 4). No characteristic textures are detected. The data obtained indicate that in the range from –96 to +120°C polymer P1 with the smallest content of rigid aromatic BTBT fragments (20%, i.e., on average in each fifth monomer unit) exists in the

Table 2. Thermal properties and phase characteristics of polymers P1–P3

Polymer	5% weight loss in gas flow, °C		Phase transition temperature (°C)/enthalpy (J/g)		
	air	nitrogen	first heating	cooling	second heating
P1	348	390	50/12, 110 /5	–	52/18, 110/6
P2	343	413	95/24, 156 /11	153/11, 84/10	95/10, 156/11
P3a	279	274	90/12, 120/5, 201/10	198/10, 109/9	118 /8, 201/10
P3b	325	404	100/14, 122/8, 195/12	193/10, 108/11	118/11, 193/10
5	296	297	79/79, 113/16	111/15, 52/48	70/51, 113/16
O(Si-Und-BTBT-Hex)$_2$ [21]	316	423	83/35, 144/18	141/17, 76/32	81/29, 144/17

For polymer P1 $T_g = -128$ and –96°C and $\Delta c_p = 0.219$ and 0.127 J/(g deg) under first and second heating, respectively.

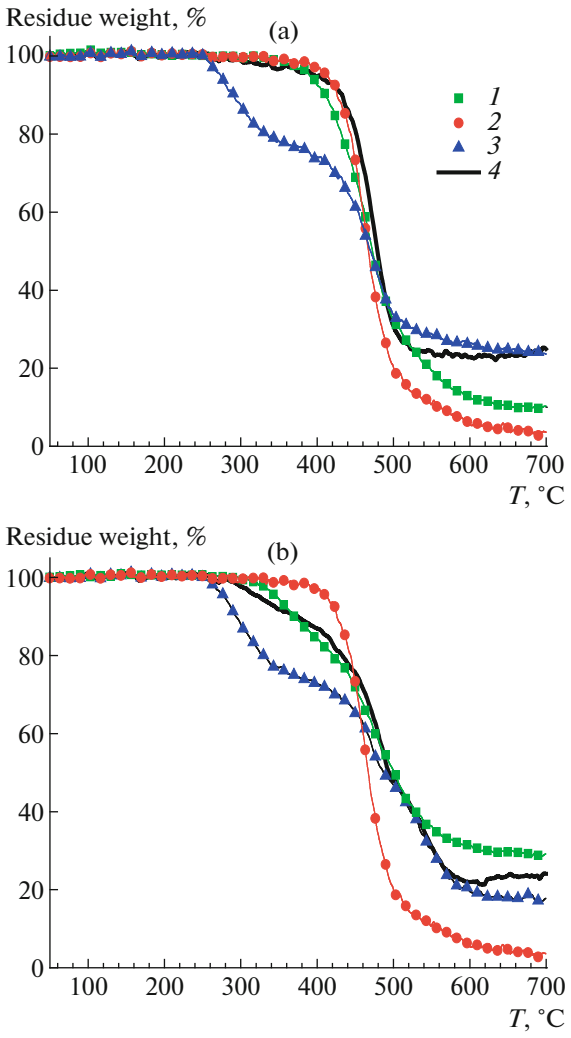

Fig. 2. TGA curves of (*1*) P1, (*2*) P2, (*3*) P3a, and (*4*) P3b polymers under heating in an atmosphere of (a) nitrogen and (b) air.

LC state associated to the interaction of BTBT fragments.

The DSC thermograms of polymer P2 show no inflections of a baseline related to the glass transition of the polymer chain. Meanwhile, two endothermic peaks manifest themselves both in the first and second heating, as well as under cooling. Compared with polymer P1 the first endothermic peak with a maximum at a temperature of 95°C is sufficiently narrow and the enthalpy is 24 and 10 J/g in the first and second heating, respectively. The second endothermic peak with a maximum at 156°C and a melting enthalpy of 11 J/g is reproduced both in the first and second heating. Upon cooling two exothermic peaks with an enthalpy of 11 and 10 J/g are observed at temperatures of 153 and 84°C. Thus, the DSC method revealed the presence of two reversible phase transitions at 95 and 156°C with the enthalpy values typical of smectic LC mesophases.

Polarizing optical microscopy studies show that polymer P2 in crossed polaroids exhibits birefringence at room temperature. The intensity of birefringence increases at 156°C, while above 180°C it disappears (Fig. 4). No characteristic textures are identified. These data indicate that for polymer P2 containing 50% of monomer units with BTBT fragments two enantiotropic LC mesophases (presumably smectic) are manifested which above 180°C transform into the isotropic melt.

Polymer P3 was separated into two fractions with different molecular weights: high molecular weight P3a and low molecular weight P3b. A comparison of the DSC thermograms of both fractions suggests that their phase behavior is similar: the second heating thermograms exhibit two exothermic peaks at 118 and 201°C (193°C for P3b) with a melting enthalpy of 8 (11 for P3b) and 10 J/g. These both phase transitions are also observed on the cooling curves which provides

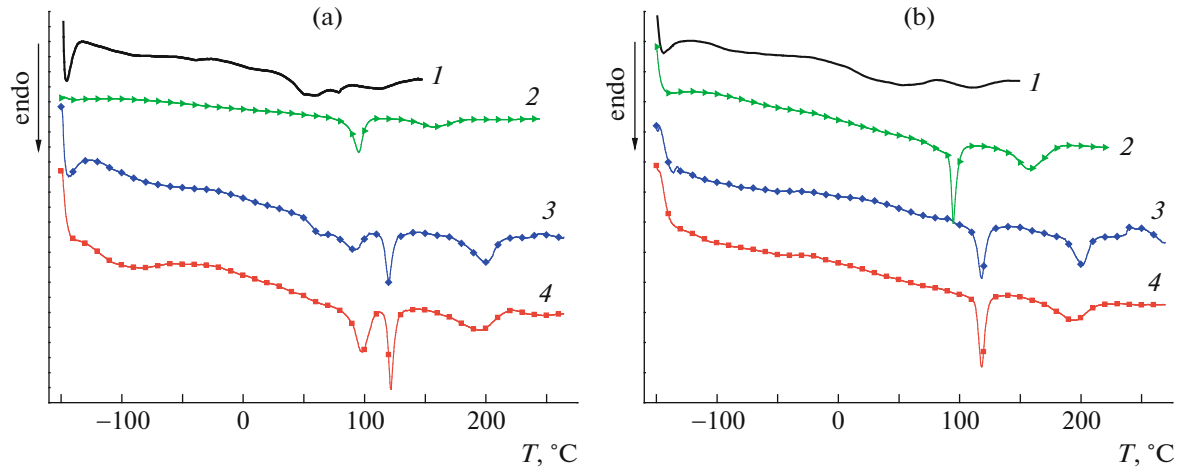

Fig. 3. DSC thermograms upon (a) first and (b) second heating of (*1*) P1, (*2*) P2, (*3*) P3a, and (*4*) P3b polymers.

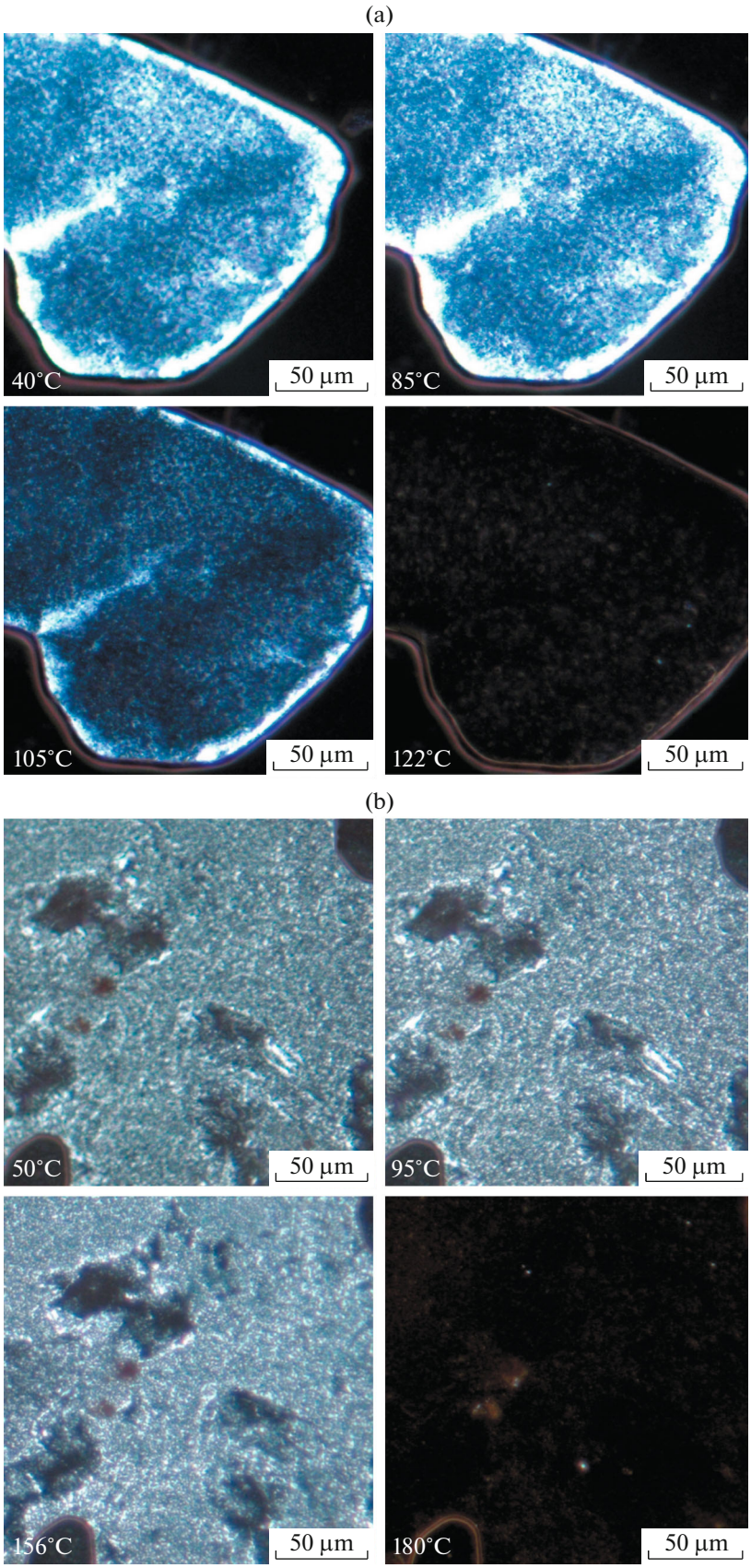

Fig. 4. Polarizing optical microphotographs of (a) P1 and (b) P2 polymers in crossed polaroids under heating.

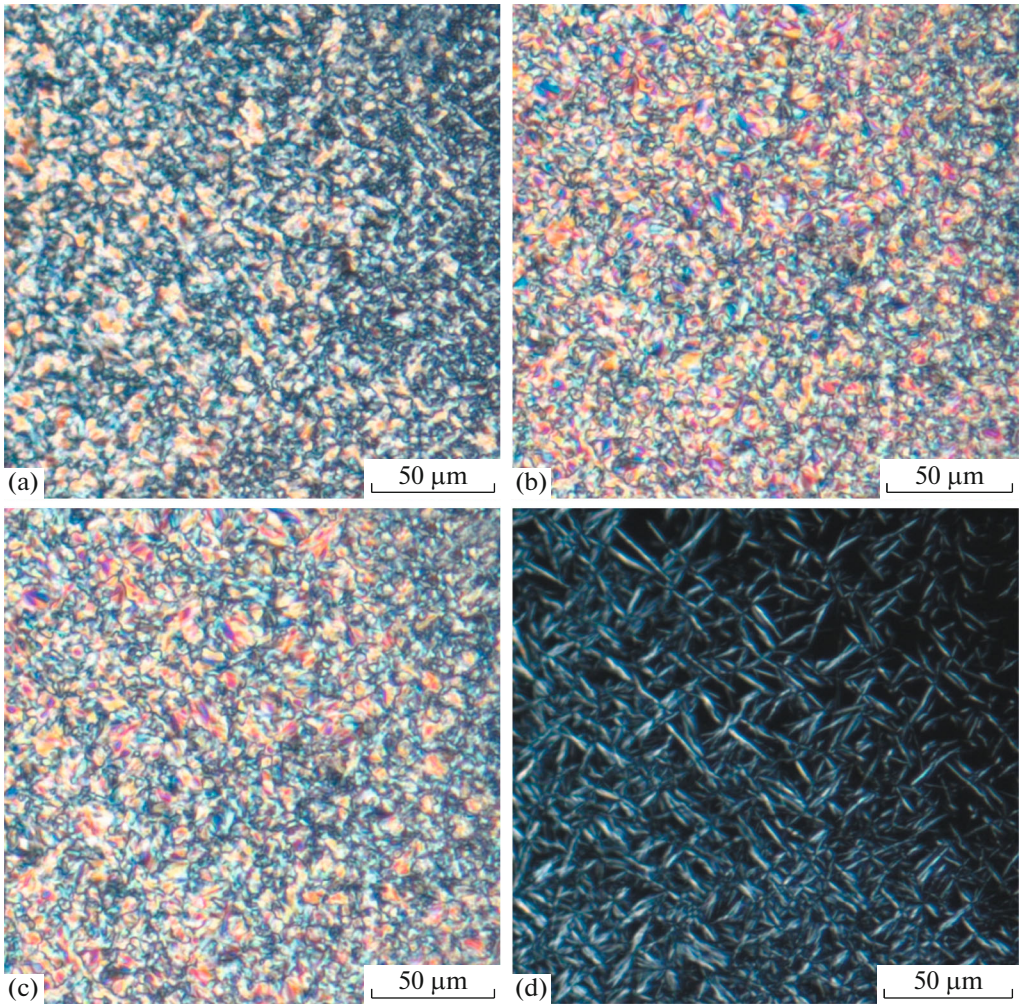

Fig. 5. Polarizing optical microphotographs of polymer P3a in crossed polaroids under (a–c) heating and (d) cooling from the isotropic melt. T = (a) 50, (b) 130, (c) 205, and (d) 220°C.

evidence for their reversibility. In addition, the first heating thermograms show lower temperature broad endothermic peaks with maxima at 90 and 100°C and an enthalpy of 12 and 14 J/g for P3a and P3b, respectively. These enthalpy values are inherent in smectic mesophases.

On the polarizing optical microphotographs of polymer P3a the Schlieren texture is seen; its color intensity slightly changes under heating (Fig. 5). Upon cooling from the isotropic melt at a temperature below 220°C "bars" typical of the smectic mesophase appear. For polymer P3b under heating the broken fan-shaped texture is detected, while after cooling below 205°C "bars" emerge which gradually transform into the broken fan-shaped texture (Fig. 6). It should be noted that both the Schlieren texture and the broken fan-shaped texture are common for the inclined smectic C mesophase [28]. However, without X-ray phase analysis the observed phase transitions cannot be unambiguously assigned to certain mesophases.

An analysis of the second heating DSC thermograms makes it possible to gain insight into dependence between the number of BTBT fragments incorporated into the polymer chain and the phase transition temperatures of the copolymers. For the initial asymmetric dialkyl derivative of BTBT (5) the DSC thermogram shows two exothermic peaks at 70 and 113°C with a melting enthalpy of 51 and 16 J/g, respectively (Table 2) [21]. On switching to the siloxane dimer O(Si-Und-BTBT-Hex)$_2$ composed of two BTBT fragments linked by undecyl spacers to the central tetramethyldisiloxane fragment the phase behavior changes: the temperature of both phase transitions grows (81 and 144°C), meanwhile the melting enthalpy of the first peak decreases to 29 J/g and the melting enthalpy of the second peak increases slightly (to 17 J/g). These changes can be explained by the fact that the weight of molecules grows by more than two

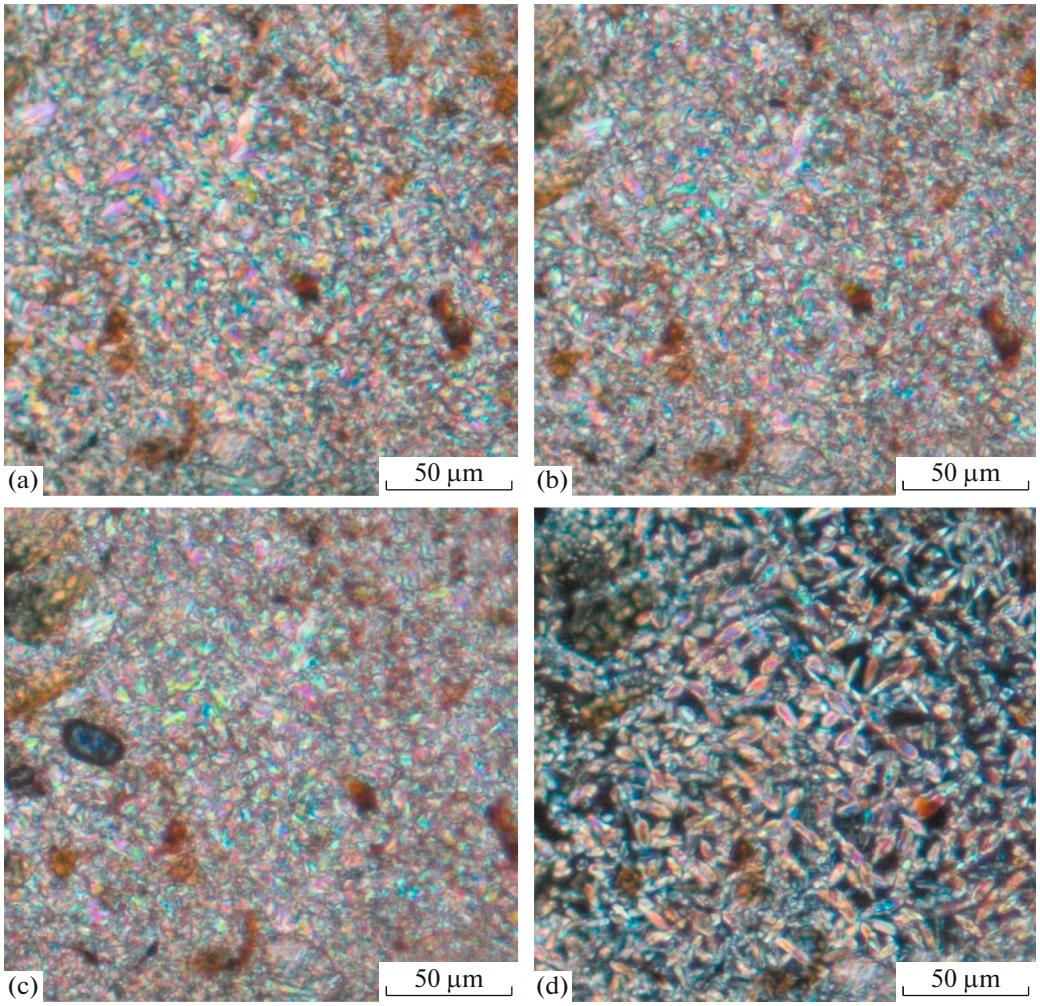

Fig. 6. Polarizing optical microphotographs of polymer P3b in crossed polaroids under (a–c) heating and (d) cooling from the isotropic melt. T = (a) 50, (b) 110, (c) 150, and (d) 205°C.

times on switching from monomer BTBT (5) to dimer O(Si-Und-BTBT-Hex)$_2$, as well as by appearance of the bulky tetramethyldisiloxane fragment in the dimer hampering crystallization. On switching to copolymer P2 containing 50% of monomer units with BTBT fragments the temperature of both phase transitions continues to grow (95 and 156°C) and the enthalpy slightly decreases to 10 and 11 J/g, respectively. On switching to polymers P3 with the 100% content of BTBT fragments in monomer units the temperatures of both phase transitions increase further: to 118 and 193°C for the low molecular weight fraction P3b and 118 and 201°C for the high molecular weight fraction P3a. Note that the enthalpy of the mentioned phase transitions changes insignificantly: 11 vs. 10 J/g for P3b and 8 vs. 10 J/g for P3a. Thus, in the sequence: monomer BTBT (5), dimer O(Si-Und-BTBT-Hex)$_2$, P2 and P3, the temperature of both phase transitions increases with increasing number of BTBT moieties. It should be emphasized that the temperature of the first phase transition is primarily affected by the fraction of BTBT fragments, while the temperature of the second phase transition is influenced by the molecular weight of a macromolecule, as is evident from comparison of the temperatures for polymers P3a and P3b. Upon the introduction of siloxane fragments into macromolecules the enthalpy of both phase transitions decreases in the sequence: 5 > O(Si-Und-BTBT-Hex)$_2$ > P2 ≈ P3a ≈ P3b.

Polymer P1 falls out from the comparison sequence because of a too high content of siloxane fragments (80%): for this polymer, the peaks of both phase transitions are very broad (several tens degrees) and their average temperatures are much lower than those for monomer 5. Thus, the incorporation of 20% of BTBT groups insignificantly changes properties of the initial PMS, as is proved by the appearance of low glass transition temperatures common for polysiloxanes on the DSC thermograms. However, upon the incorporation of 50 and 100% of BTBT fragments into

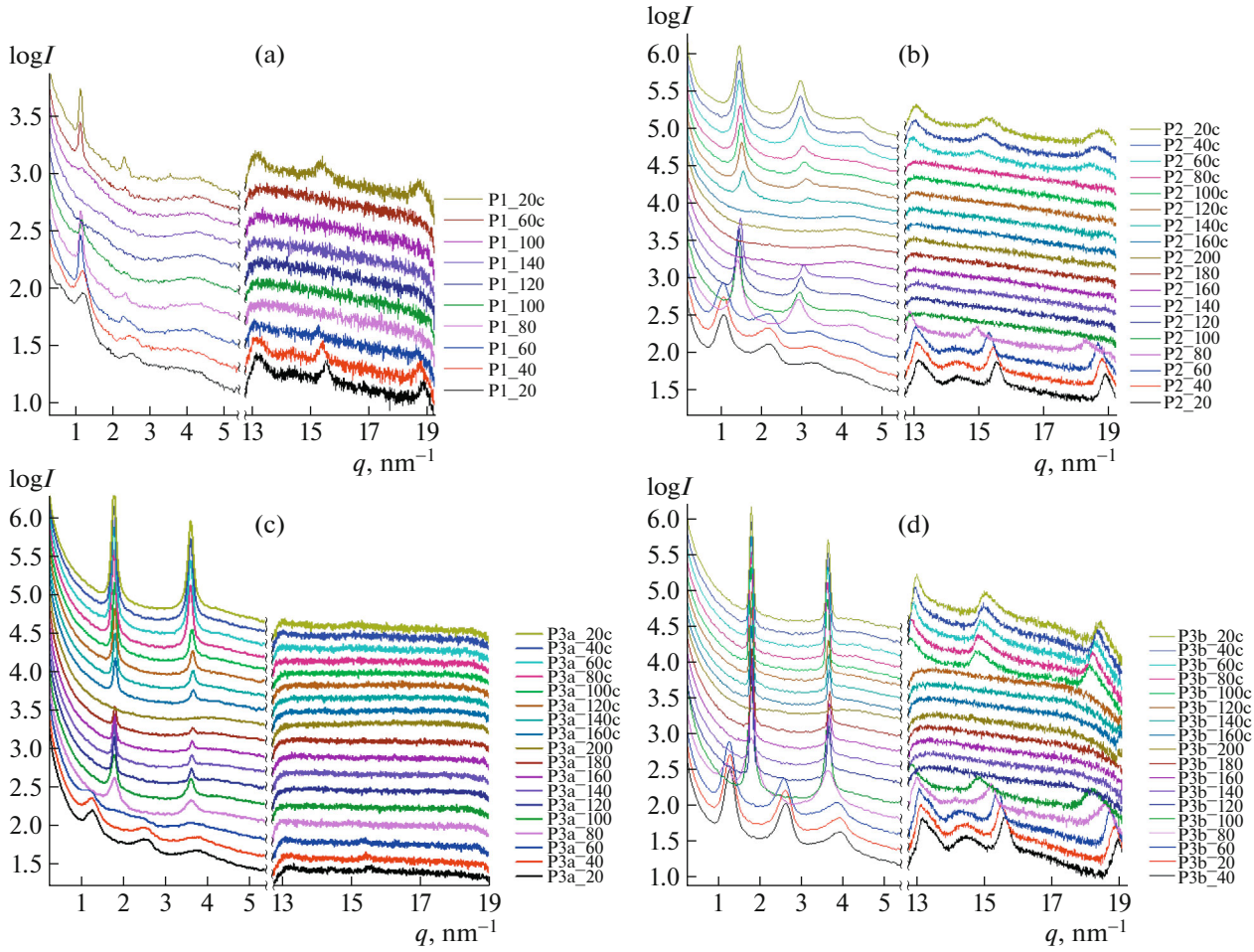

Fig. 7. Small- and wide-angle X-ray diffraction patterns of (a) P1, (b) P2, (c) P3a, and (d) P3b polymers under heating from room temperature to 200°C followed by cooling. The intensity is given in the logarithmic scale, and the curves are shifted along the vertical.

the monomer units of copolymers P2 and P3 well-defined peaks of phase transitions typical of BTBT derivatives manifest themselves [5], melting temperatures increase, and liquid-crystalline mesophases with textures and melting enthalpies inherent in smectic mesophases appear.

To determine the structure and phase behavior of the synthesized polymers small-angle and wide-angle X-ray diffraction patterns were measured at varying temperature of the sample. Dialkyl-substituted BTBT derivatives (C_n-BTBT-C_m) are known to be subject to crystallization into the monoclinic type lattice [5], with axis c being directed at an angle to aliphatic and conjugated fragments and leading to emergence of a set of 001 reflections in the small-angle range. At the same time, reflections hk0 are often manifested in the wide-angle range, suggesting formation of the herringbone-type packing.

For P1 (Fig. 7a) at room temperature two small-angle reflections 001 and 002 attributed to the layer packing were observed. In the wide-angle range, three weak reflections at q = 13.3, 15.5, and 18.8 nm^{-1} were also detected. Upon heating to 60°C the wide-angle reflections disappeared and simultaneously the half-width of small-angle peaks decreased, which corresponded to transition to the smectic mesophase with enlarged domains. The interlayer spacing in the smectic phase slightly increased from 5.2 to 5.6 nm. Further heating resulted in the appearance of transition to the isotropic state, while cooling restored the initial phase.

The X-ray diffraction patterns of P2 (Fig. 7b) at room temperature display a number of small-angle reflections corresponding to a period of 5.8 nm, as well as clear wide-angle reflections with interplanar spacings similar to those of P1. Heating above 60°C resulted in the phase transition to the smectic phase with a parameter of 4.4 nm and a simultaneous loss of wide-angle reflections. The obtained smectic phase transformed into the isotropic state at a temperature above 140°C and restored upon subsequent cooling. Wide-angle reflections were recovered at a tempera-

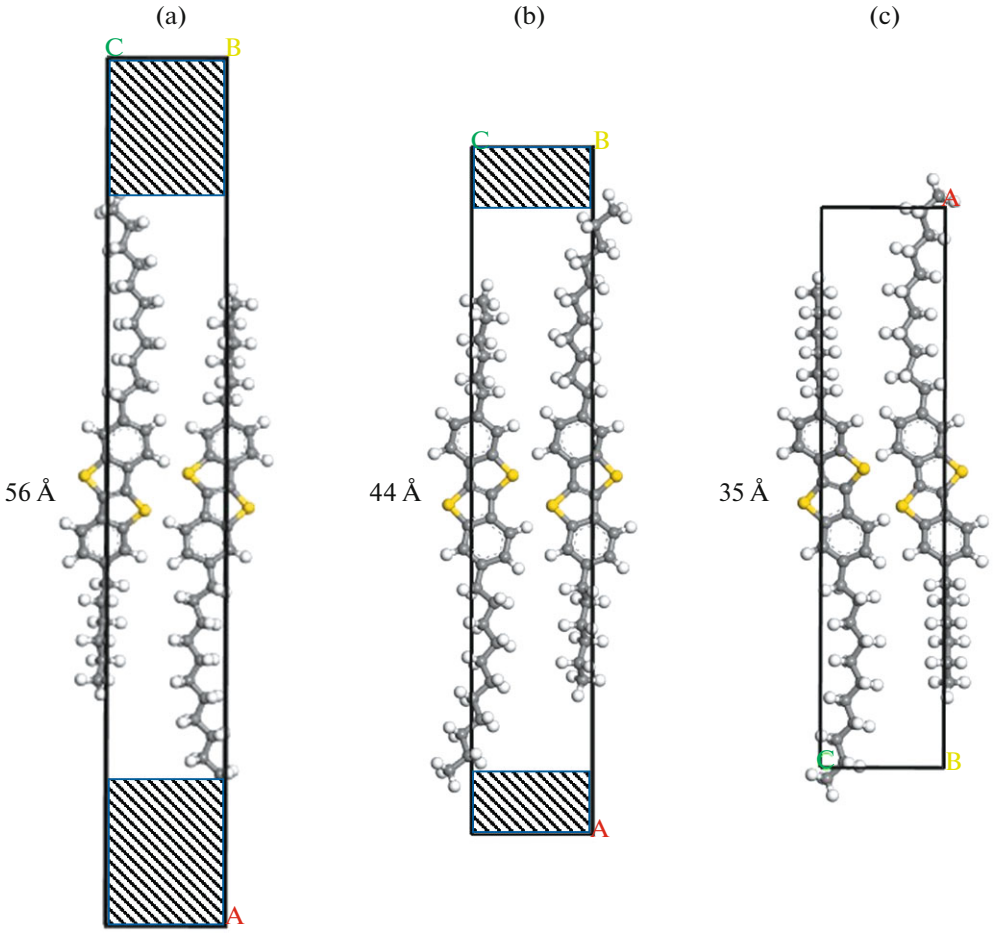

Fig. 8. Proposed changes in the type of packing of BTBT fragments for (a) P1, (b) P2, and (c) P3 polymers in the cooled state. Parameters of the smectic phase c are given, and the lateral parameters are assumed to be $a = 5.86$ and $b = 7.74$, which are typical values for the packing of dialkyl-substituted BTBTs. Cross-hatched areas mark the polysiloxane location.

ture below 80°C. The initial nascent crystalline phase was not restored.

For P3a and P3b (Fig. 7c, 7d), which are different fractions of the same polymer, small-angle X-ray scattering pictures are similar, namely, a set of broad reflections with a period of 4.9 nm. However, for P3a with a high molecular weight wide-angle reflections are absent, in contrast to P3b. Thus, lengthening of the flexible polymer chain hampers formation of the lateral conjugated packing. The position of wide-angle reflections for P3b is similar to that for P1 and P2. Heating above 60°C leads to the irreversible transition to the smectic phase with a parameter of 3.5 nm for both samples; however, in the case of P3b wide-angle reflections disappear only at temperatures above 100°C, which is consistent with the DSC data (the double peak in the range of 90–120°C). The reversible transition to the isotropic phase is observed above 180°C, and cooling facilitates recovery of the smectic phase with a parameter of 3.5 nm, while wide-angle reflections in P3b appear at a temperature below 120°C. The nascent phase, as in P2, is not restored under cooling to room temperature.

Thus, the X-ray diffraction data allow the following conclusions to be made. First, with an increase in the content of BTBT fragments to 50% or above the nascent phase appears and is not restored upon subsequent cooling. Hence, the data obtained under cooling are more important for comparison and analysis of the phase behavior. Second, an increase in molecular weight causes the loss of lateral crystalline packing and interaction of conjugated BTBT moieties. Third, even though the type of BTBT fragments is preserved, an increase in their content causes a considerably change in the interlayer spacing, while the type of packing remains unchanged. The proposed packing models are shown in Fig. 8, which clearly illustrates a change in the depth of interpenetration of side substituents with an increase in their concentration. For example, using the values of the interlayer spacing for P1 it can be assumed that only hexyl fragments overlap. For P2 the interlayer spacing decreases appreciably, indicating

the approach of aromatic groups of neighboring chains. For compounds P3a and P3b the interlayer spacing is close to the complete length of the substituent, disregarding the slope of alkyl and conjugated groups to axis *c*, which corresponds to the complete interpenetration of side fragments. For O(Si-Und-BTBT-Hex)$_2$ the d-spacing in the condensed state is 3.58 nm, which is close to the packing parameters of P3a and P3b and optimal for dialkyl-substituted BTBT derivatives, such as C11-BTBT showing 3.59 nm [5].

CONCLUSIONS

A number of novel polysiloxanes modified with dialkyl derivatives of BTBT through the hydrosilylation of (co)polysiloxanes with various content of Si–H groups in monomer units (20, 50, and 100%) has been synthesized. It is found that, in the synthesis of the BTBT-containing precursor, during reduction of the keto group by $LiAlH_4$ in diethyl ether, along with the target reaction, the reaction of dibromide deprotection occurs to form the end double bond which considerably accelerates the process. The chemical structure of the synthesized macromolecules is confirmed by ^{1}H NMR spectroscopy, and their molecular weight distribution is characterized by GPC. The synthesized polymers have a number-average molecular weight of (6–43) × 10^3 and a dispersity of 1.55–2.79.

The study of thermal and thermo-oxidative properties of the synthesized compounds has demonstrated that polymer P2, in which each second monomer unit contains BTBT substituents, possesses the highest thermo-oxidative stability (413°C) and the smallest char residue at 700°C (3%). Polymer P3a containing 100% of BTBT fragments and having the highest molecular weight is the less thermally stable: for this polymer the 5% weight loss is observed at 274°C.

Investigation of the phase behavior of the copolymers by DSC and polarizing optical microscopy has revealed that in the range from –96 to 120°C polymer P1 containing 20% of rigid BTBT fragments occurs in the LC state. The introduction of 50 and 100% of BTBT fragments into the siloxane polymer chain gives rise to the LC mesophase with the enthalpy characteristic of smectic mesophases. It is shown that with an increase in the content of BTBT fragments the phase transition temperature of polymers P2, P3a, and P3b grows. The introduction of siloxane fragments into macromolecules decreases the enthalpy of both phase transitions in the sequence: monomer BTBT (5) > dimer O(Si-Und-BTBT-Hex)$_2$ > P2 ≈ P3a ≈ P3b.

The X-ray diffraction data has made it possible to determine the smectic packing of compounds, to evaluate the dependence of packing parameters on the content of BTBT, and to propose the packing model of side substituents. It is shown that nascent phases and phase transitions corresponding to the loss of lateral ordering exist and the values of transition temperatures are consistent to those derived from the DSC data.

The phase behavior of the synthesized polymers with a high content of BTBT fragments suggests that they show promise for application in organic electronic devices. This will be the subject of our further studies.

ACKNOWLEDGMENTS

We are grateful to the Collaborative Access Center for Polymer Research Center of the Enikolopov Institute of Synthetic Polymer Materials, Russian Academy of Sciences under support of the Ministry of Science and Higher Education of the Russian Federation (theme no. FFSM-2021-0005) for GPC analysis and molecular weight studies and P.V. Dmitraykov for TGA and DSC measurements.

FUNDING

This work was supported by the Russian Science Foundation (project no. 19-73-30028).

CONFLICT OF INTEREST

The authors declare that they have no conflicts of interest.

REFERENCES

1. H. Jiang, S. Zhu, Z. Cui, Z. Li, Y. Liang, J. Zhu, P. Hu, H.-L. Zhang, and W. Hu, Chem. Soc. Rev. **51**, 3071 (2022).
2. A. S. Sizov, E. V. Agina, and S. A. Ponomarenko, Russ. Chem. Rev. **87** (12), 1226 (2018).
3. P. A. Shaposhnik, S. A. Zapunidi, M. V. Shestakov, E. V. Agina, and S. A. Ponomarenko, Russ. Chem. Rev. **89** (12), 1483 (2020).
4. A. A. Trul, E. V. Agina, and S. A. Ponomarenko, Polym. Sci., Ser. B **63** (5), 443 (2021).
5. H. Ebata, T. Izawa, E. Miyazaki, K. Takimiya, M. Ikeda, H. Kuwabara, and T. Yui, J. Am. Chem. Soc. **129** (51), 15732 (2007).
6. P. Xie, T. Liu, J. Sun, and J. Yang, Adv. Funct. Mater, 2200843 (2022).
7. J. Li, A. Babuji, I. Temino, T. Salzillo, F. D'Amiso, R. Pfattner, S. Osal, E. Barrena, and M. Mas-Torrent, Adv. Mater. Technol., 2101535 (2022).
8. I. Temino, F. G. Del Pozo, M. R. Ajayakumar, S. Galindo, J. Puigdollers, and M. Mas-Torrent, Adv. Mater. Technol., 1600090 (2016).
9. T. Shen, H. Zhou, J. Xin, Q. Fan, Z. Yang, J. Wang, T. Mei, X. Wang, N. Wang, and J. Li, Appl. Surf. Sci. **498**, 143822 (2019).
10. M. Zhang, J. Wu, H. Lin, X. Zhang, J.-L. Xu, Y. Ya, S.-D. Wang, M. Wong, and H.-S. Kwok, Electron Device Lett. **42** (7), 998 (2021).
11. Y. Wang, S. Meijia, K. Xin, W. Xiangjian, and Y. Guangsheng, Polymer **185**, 121976 (2019).

12. Z. Zhijie, D. Jiamin, Y. Linglong, W. Guo, Z. Bin, T. Songting, S. Ping, H. S. Ryu, W. H. Young, and S. Yanming, J. Mater. Chem. A **8**, 9684 (2020).
13. G. H. Roche, G. Bruckner, D. G. Dumitrescu, J. J. E. Moreau, A. van der Lee, G. Wantz, and O. J. Dautel, Adv. Electron. Mater. **8**, 2100265 (2022).
14. G. Christos, N. Slaude, R. Christian, Y. H. Geerts, and G. Floudas, J. Phys. Chem. B **118** (5), 1443 (2014).
15. S. P. Prakoso, Y.-J. Ke, D.-S. Huang, S.-L. Wang, and Y.-T. Tao, J. Chin. Chem. Soc. **6** (3), 440 (2022).
16. Y. Dong, Y. Sun, J. Liu, X. Shi, H. Li, J. Zhang, S. Li, Y. Yi, S. Mo, L. Fan, and L. Jiang, Adv. Sci. **9**, 2106085 (2022).
17. A. Tamayo, S. Hofer, T. Salzillo, C. Ruzie, R. Resel, and M. Mas-Torrent, J. Mater. Chem. C **9**, 7186 (2021).
18. W. Shin, M. Y. Jo, D. S. You, Y. S. Jeong, D. Y. Yoon, J.-W. Kang, J. H. Sho, G. D. Lee, S.-S. Hong, and J. H. Kim, Synth. Met. **162** (9–10), 768 (2012).
19. S. K. Samanta, I. Song, J. H. Yoo, and J. H. Oh, ACS Appl. Mater. Interfaces **10** (38), 32444 (2018).
20. V. S. Nair, Jibin Sun, P. Qi, S. Yang, Z. Liu, D. Zhang, and A. Ajayaghosh, Macromolecules **49** (17), 6334 (2016).
21. O. V. Borshchev, A. S. Sizov, E. V. Agina, A. A. Bessonov, and S. A. Ponomarenko, Chem. Commun. **53**, 885 (2017).
22. A. A. Trul, V. P. Chekusova, D. S. Anisimov, O. V. Borshchev, M. S. Polinskaya, E. V. Agina, and S. A. Ponomarenko, Adv. Electron. Mater. **8**, 2101039 (2022).
23. A. A. Trul, A. S. Sizov, V. P. Chekusova, O. B. Borshchev, E. V. Agina, M. A. Shcherbina, A. V. Bakirov, S. N. Chvalun, and S. A. Ponomarenko, J. Mater. Chem. **6**, 9649 (2018).
24. V. V. Gorodov, N. V. Demchenko, and M. I. Buzin, Russ. Chem. Bull. **66**, 1290 (2017).
25. F. Osterod, L. Peters, A. Kraft, T. Sano, J. J. Morrison, N. Feeder, and A. B. Holmes, J. Mater. Chem. **11**, 1625 (2001).
26. S. A. Ponomarenko, O. V. Borshchev, T. Meyer-Friedrishsen, A. P. Pleshkova, S. Setayesh, E. S. P. Smits, S. G. J. Mathijssen, D. M. de Leeuw, S. Kirchmeyer, and A. M. Muzafarov, Organometallics **29** (19), 4213 (2010).
27. P. A. Klonos, Polymer **159**, 169 (2018).
28. I. Dierking, *Textures of Liquid Crystals* (Wiley-VSH, Weinheim, 2003).

Translated by T. Soboleva